

## Confinement effects on the properties of Janus dimers

José Rafael Bordin<sup>1, a)</sup> and Leandro B. Krott<sup>2</sup>

<sup>1)</sup>*Campus Caçapava do Sul, Universidade Federal do Pampa,  
Av. Pedro Anunciação 111, CEP 96570-000, Caçapava do Sul,  
Brazil. E-mail: josebordin@unipampa.edu.br*

<sup>2)</sup>*Centro Araranguá, Universidade Federal de Santa Catarina,  
Rua Pedro João Pereira, 150, CEP 88905-120, Araranguá, SC,  
Brazil. E-mail: leandro.krott@ufsc.br*

Confinement has been suggested as a tool to tune the self-assembly properties of nanoparticles, surfactants, polymers and colloids. In this way, we explore the phase diagram of Janus nanoparticles using Molecular Dynamics simulations. The nanoparticle was modeled as a dimer made by one monomer that interacts by a standard Lennard Jones potential and another monomer that is modeled using a two-length scale shoulder potential. This specific design of nanoparticle exhibits in bulk distinct self-assembled structures and water-like diffusion anomaly. Our results indicate that besides the aggregates observed in bulk, new structures are observed under confinement. Also, the dynamic and thermodynamic behavior of the fluid phase are affected. The systems show a reentrant fluid phase and density anomaly. None of these two features were observed in bulk. Our results show that geometrical confinement leads to new structural, thermodynamical and dynamical behavior for this Janus nanoparticle.

---

<sup>a)</sup>Electronic mail: josebordin@unipampa.edu.br

## I. INTRODUCTION

Colloids and molecules with anisotropic shapes and interactions play a significant role in condensed matter physics, specially in the design of self-assembled structures<sup>1,2</sup>. Particularly, Janus colloids are characterized as particles composed by at least two physically or chemically distinctive surfaces. They can have different shapes, as rods, spheres and dumbbells. These systems have a large range of applications including medicine, self-driven molecules, catalysis, photonic crystals, stable emulsions, biomolecules and self-healing materials<sup>3-11</sup>.

From the distinct Janus particles shapes, Janus dumbbells<sup>12-15</sup> are colloids formed by two spheres, each one with distinct characteristics linked together with a separation that varies from an almost total overlap to one or two monomer diameters. Due to the resemblance between Janus particles and competing interaction systems, Janus dumbbells behave as surfactant in water-based emulsions due its amphiphilic properties<sup>16-18</sup>. Self-assembly lamellae or micellae phases were observed on these systems due the competition between attractive and repulsive forces<sup>19-24</sup>.

Recent studies reported the production of silver-silicon (Ag-Si)<sup>13</sup> and silica-polystyrene (SiO<sub>2</sub>-PS)<sup>25</sup> Janus dimers. Silica and silicon are classified as anomalous fluids, and therefore have a set of properties that diverge from the observed for regular materials. For most part of the fluids, the diffusion coefficient decreases when the pressure (or density) increases. However, materials as water<sup>26</sup>, silicon<sup>27</sup> and silica<sup>28</sup> show diffusion anomaly, characterized by a maximum in the diffusion coefficient at constant temperature. Besides diffusion (or dynamical) anomaly, water, silicon, silica and others fluids, the so-called anomalous fluids, also have other classes of anomalies, as structure and thermodynamic anomalies. Particularly, the density anomaly is characterized by the increase of density with the temperature at a fixed pressure.

Distinct computational models were proposed to study the anomalous behavior of fluids. Among these models, effective two length scale (TLS) core-softened shoulder potential are an interesting tool to investigate systems with water-like anomalies. Particularly, the model proposed by Oliveira *et. al.*<sup>29,30</sup> reproduces qualitatively the diffusion, structural and thermodynamic anomalies, and was broadly used to study anomalous systems. This effective approach to describe anomalous fluids was used to study monomeric and dimeric systems of anomalous particles<sup>29-33</sup>. The TLS potential was used in our previous works to study the

behavior of Janus dumbbells composed of one anomalous and one non-anomalous monomers in bulk<sup>34,35</sup>. Despite the presence of the non-anomalous monomer, the diffusion anomaly was preserved.

Confinement was proposed as a approach to tune the self-assembled morphologies. Controlling the confinement intensity it is possible to create micelles with distinct shapes. Computational and experimental studies have already explore the confinement effects if the self assembly of polyhedral nanoparticles<sup>36</sup>, patchy spherical colloids<sup>37</sup>, asymmetric and symmetric dumbbells<sup>38,39</sup> surfactants and polymers<sup>40–42</sup>. As well, the confinement affects the diffusivity of spherical Janus swimmers<sup>11</sup>. In fact, confinement strongly affects the behavior of fluids in general. For the case of anomalous fluids<sup>43</sup>, new anomalies can be observed due confinement<sup>44</sup>, and even a superdiffusive regime can be induced<sup>45</sup>. The anomalous region in the pressure  $\times$  temperature ( $PT$ ) phase diagram is usually shifted due confinement. This shift can be to higher or lower temperatures, regarding on the nature of the fluid-wall interaction<sup>46</sup>.

Therefore, the question that rises is how the confinement will affect not only the self-assembled structures, but the dynamical and thermodynamical behavior of the anomalous/non-anomalous Janus dumbbell system. In this way, we perform intensive Molecular Dynamics (MD) simulations of Janus nanoparticles composed of anomalous and non-anomalous monomers confined between two flat plates. In addition to the myriad of structures tuned by the confinement, we show how the confinement and the TLS potential lead the system to have not only diffusion anomaly, but also the density anomaly, not observed in bulk.

The paper is organized as follows: first we introduce the model and describe the methods and simulation details; next the results and discussion are given; and then we present our conclusions.

## II. THE MODEL AND THE SIMULATION DETAILS

In this paper all physical quantities are computed in the standard Lennard Jones (LJ) units<sup>47</sup>,

$$r^* \equiv \frac{r}{\sigma}, \quad \rho^* \equiv \rho\sigma^3, \quad \text{and} \quad t^* \equiv t \left( \frac{\epsilon}{m\sigma^2} \right)^{1/2}, \quad (1)$$

for distance, density of particles and time, respectively, and

$$p^* \equiv \frac{p\sigma^3}{\epsilon} \quad \text{and} \quad T^* \equiv \frac{k_B T}{\epsilon} \quad (2)$$

for the pressure and temperature, respectively, where  $\sigma$ ,  $\epsilon$  and  $m$  are the distance, energy and mass parameters, respectively. Since all physical quantities are defined in reduced LJ units, the  $*$  is omitted, in order to simplify the discussion.

The systems have  $N = 1000$  dimeric particles, totalizing  $N = 2000$  particles, confined between two smooth and parallel plates. The Janus dumbbells particles were modeled using two spherical core-softened particles, each one with mass  $m$  and effective diameter  $\sigma$ , linked rigidly at a distance  $\lambda$ . The dimers are formed by monomers of type A and type B.

The particles of type A present anomalous behavior and their interaction is given by a two length scales potential, potential AA, defined as<sup>29,30</sup>

$$\begin{aligned} \frac{U^{AA}(r_{ij})}{\epsilon} = & 4 \left[ \left( \frac{\sigma}{r_{ij}} \right)^{12} - \left( \frac{\sigma}{r_{ij}} \right)^6 \right] + \\ & u_0 \exp \left[ -\frac{1}{c_0^2} \left( \frac{r_{ij} - r_0}{\sigma} \right)^2 \right], \end{aligned} \quad (3)$$

where  $r_{ij} = |\vec{r}_i - \vec{r}_j|$  is the distance between two A particles  $i$  and  $j$ . The first term of the potential is a standard 12-6 LJ potential<sup>47</sup> and the second one is a Gaussian shoulder centered at  $r_0$ , with depth  $u_0$  and width  $c_0$ . The parameters used in this work are  $u_0 = 5.0$ ,  $c_0 = 1.0$  and  $r_0/\sigma = 0.7$ . Both systems, monomeric and dimeric, modeled by this potential, present density, diffusion and thermodynamic anomalies, like observed in water, silica and other anomalous fluids<sup>29-31,48,49</sup>.

The interaction between particles of type B, the potential BB, is given by a standard 12-6 LJ potential, like the first term of Eq. 3, cut and shifted at the cutoff radius  $r_c$ ,

$$U^{\text{CSLJ}}(r_{ij}) = \begin{cases} U_{\text{LJ}}(r_{ij}) - U_{\text{LJ}}(r_c), & r_{ij} \leq r_c, \\ 0, & r_{ij} > r_c. \end{cases} \quad (4)$$

The BB potential has a cutoff radius of  $r_c = 2.5$ . Meanwhile, the interaction for A-B particles is given by the Weeks-Chandler-Andersen (WCA) potential, defined by the equation 4 with  $r_c = 2^{1/6}$  is the cutoff. The interactions between dimers and walls are given by the projection of the WCA potential in the  $z$ -direction. The potentials are illustrated in Fig. 1.

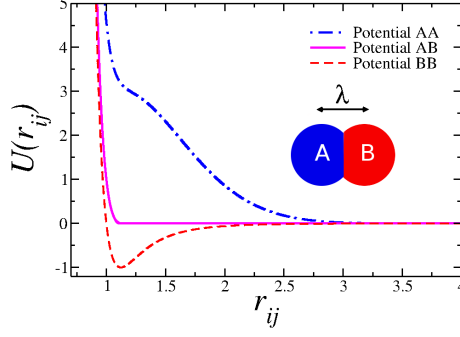


FIG. 1. Interaction potential between particles of type A (dot-dashed blue line), between particle of type A and B (solid magenta line) and between particles of type B (dashed red line). The interaction between dimers and confining walls is given by the projection of the potential AB in  $z$ -direction. Inset: Janus dumbbells formed by A-B monomers.

The simulations were performed in the canonical ensemble using the ESPResSo package<sup>50,51</sup>. The number density, defined as  $\rho = N/V$ , where  $V = L^2 \times L_z$  is the volume of the simulation box, was varied from  $\rho = 0.05$  to  $\rho = 0.50$ . In all simulations,  $L_z = 4.0$  and  $L$  was obtained from  $L = [N/(\rho L_z)]^{1/2}$ . Standard periodic boundary conditions are applied in  $x$  and  $y$ -directions. The temperature was simulated in the interval between  $T = 0.05$  and  $T = 0.60$ . The system temperature was fixed using the Langevin thermostat with  $\gamma = 1.0$ , and the equations of motion for the fluid particles were integrated using the velocity Verlet algorithm, with a time step  $\delta t = 0.01$ . We performed  $1 \times 10^6$  steps to equilibrate the system. These steps are then followed by  $5 \times 10^6$  steps for the results production stage. To ensure that the system was equilibrated, the pressure, kinetic energy and potential energy were analyzed as function of time, as well several snapshots at distinct simulation times. Since confined systems can be sensitive to the number of particles in the simulation, in some points we carried out simulations with 5000 and 10000 particles, and essentially the same results were observed. As well, we run some points with a production time of  $1 \times 10^8$  to test if the system was well equilibrated, and the same results were obtained.

The system dynamics was analyzed using the lateral mean square displacement (LMSD) as function of time, given by

$$\langle [\vec{r}_{\parallel \text{cm}}(t) - \vec{r}_{\parallel \text{cm}}(t_0)]^2 \rangle = \langle \Delta \vec{r}_{\parallel \text{cm}}(t)^2 \rangle, \quad (5)$$

where  $\vec{r}_{\parallel\text{cm}}(t_0) = (x_{\text{cm}}(t_0)^2 + y_{\text{cm}}(t_0)^2)$  and  $\vec{r}_{\parallel\text{cm}}(t) = (x_{\text{cm}}(t)^2 + y_{\text{cm}}(t)^2)$  denote the parallel coordinate of the nanoparticle center of mass (cm) at a time  $t_0$  and at a later time  $t$ , respectively. The LMSD is related to the lateral diffusion coefficient,  $D_{\parallel}$ , by

$$D_{\parallel} = \lim_{t \rightarrow \infty} \frac{\langle \Delta \vec{r}_{\parallel\text{cm}}(t)^2 \rangle}{4t} . \quad (6)$$

The pressure in confined systems by parallel plates is divided in parallel and perpendicular direction. The parallel pressure,  $P_{\parallel}$ , was obtained from

$$P_{\parallel} = 0.5(\sigma_{xx} + \sigma_{yy}) ,$$

where  $\sigma_{xx}$  and  $\sigma_{yy}$  are the normal stress in the  $x$  and  $y$  direction.

The system structure was analyzed with the lateral radial distribution function (LRDF)  $g_{\parallel}(r)$ , defined as<sup>52</sup>

$$g_{\parallel}(r) \equiv \frac{1}{\rho^2 V} \sum_{i \neq j} \delta(r - r_{ij}) \left[ \theta \left( |z_i - z_j| + \frac{\delta z}{2} \right) - \theta \left( |z_i - z_j| - \frac{\delta z}{2} \right) \right] , \quad (7)$$

where  $\delta(x)$  is the Dirac  $\delta$  function and the Heaviside function  $\theta(x)$  restricts the sum of particle pair in the same slab of thickness  $\delta z = \sigma$ . The lateral radial distribution function is proportional to the probability of finding a particle at a distance  $r$  from a referent particle inside the slab of thickness  $\delta z$ .

In order to check if the Janus system shows density anomaly we evaluate the temperature of maximum density (TMD). Using thermodynamical relations, the TMD can be characterized by the minimum of the pressure versus temperature along isochores,

$$\left( \frac{\partial P_{\parallel}}{\partial T} \right)_{\rho} = 0 . \quad (8)$$

Confinement effects on the properties of Janus dimers The fluid, micellar and aggregated regions in the  $P_{\parallel}T$  phase diagrams were defined analyzing the snapshots of the systems, the lateral diffusion coefficient,  $D_{\parallel}$ , and the lateral radial distribution function,  $g_{\parallel}(r)$ . To define the nanoparticles in the same aggregate we defined a minimal distance equals to  $r_{\min} = 1.2$ . If the distance between one monomer of one dimer and a monomer of a distinct dimer is smaller than  $r_{\min}$  then both dimers belong to the same cluster.

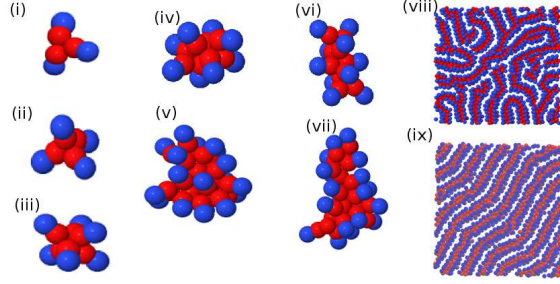


FIG. 2. Aggregates observed in our simulations: (i) trimeric cluster with  $n_c = 3$ , (ii) tetrahedral cluster with  $n_c = 4$ , (iii) hexahedral cluster with  $n_c = 6$ , (iv) spherical cluster with  $n_c = 8$ , (v) spherical cluster with  $n_c = 19$ , (vi) elongated cluster with  $n_c = 10$ , (vii) elongated cluster with  $n_c = 20$ , (viii) disoriented rippled lamellae and (ix) oriented rippled lamellae. Blue particles are the A monomers and red the B monomers.

### III. RESULTS AND DISCUSSION

We start our discussion showing the distinct micelles observed for the confined system. Regarding the temperature and density, the Janus dimers aggregate in clusters with distinct number of nanoparticles per cluster,  $n_c$ . At lower densities, trimeric clusters, with  $n_c = 3$  nanoparticles in each aggregate and tetrahedral clusters, with  $n_c = 4$ , are more common. Increasing the density, hexahedral clusters ( $n_c = 6$ ) are observed, as well spherical and elongated micelles with distinct  $n_c$ . The shape of each aggregate is shown in figure 2. For densities up to a threshold a coexistence of two or three of these micelles was observed. Above the threshold, one single rippled lamellae cluster with all the nanoparticles is observed. This lamellae phase can have a disoriented structure, as shown in figure 2(viii), or an oriented structure, figure 2(ix).

The region of micelles coexistence and the threshold to the lamellae phase depend on the temperature, so let's take the example of  $T = 0.10$ . In figure 3, we show the mean number of dimers in each cluster,  $\langle n_c \rangle$ , as function of the system density. We can establish a relation between  $\langle n_c \rangle$  and the type of aggregates. For  $0.05 < \rho \leq 0.10$ ,  $\langle n_c \rangle$  varies between 4 and 5. Analyzing the system snapshots, for these densities we can see a coexistence of trimeric, tetrahedral and hexahedral clusters. As  $\rho$  increases, more hexahedral aggregates and less trimeric aggregates are observed in the solution. This region, with the coexistence

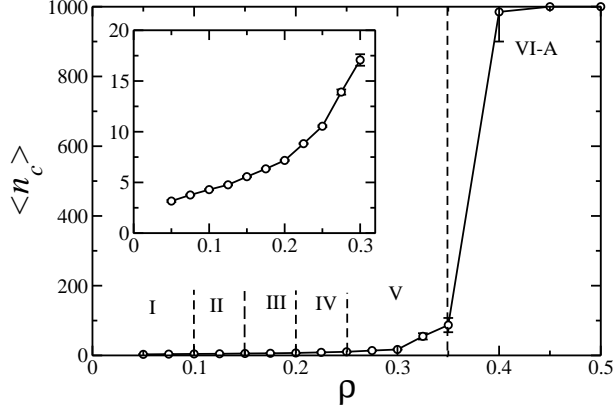


FIG. 3. Mean number of dimers in each cluster,  $\langle n_c \rangle$ , as function of density for  $T = 0.10$ . Inset: zoom in the region  $\rho < 0.30$ . Errors bars smaller than the data point are not shown.

of trimeric, tetrahedral and hexahedral clusters was labeled as region I in the figure 3. For the densities inside the region II we observe a mixture of tetrahedral and hexahedral clusters, in region III hexahedral and small spherical clusters and in region IV a coexistence of small spherical and elongated clusters. All these previous aggregates were observed in the bulk simulation, with a similar  $\langle n_c \rangle$ <sup>34</sup>. However, the confinement frustrates the self-assembly as the density increases. Therefore, if for lower densities the system aggregates in the same micelles observed for the bulk case, for higher densities new kinds of self-assembled aggregates should be induced by the confinement. In this way, the spherical and elongated micelles can have a higher  $\langle n_c \rangle$  compared to the bulk case. Basically, the limited space induced by the confinement leads two or more smaller micelles to merge in a large cluster. This region, with spherical and elongated micelles formed by more nanoparticles than the observed in bulk was labeled region V. The size of the micelles grows continually up to  $\rho = 0.35$  for  $T = 0.10$ , with approximately 10 aggregates with 100 nanoparticles each, as shown in figure 3, and above this threshold all the particles aggregate in a lamellae structure, region VI-A of figure 3. For the temperature  $T = 0.10$  and  $\rho > 0.40$ , the rippled lamellae is disoriented, without a preferable direction, as we shown in figure 2(viii). However, for some values of temperatures and densities, as  $T = 0.25$  and  $\rho = 0.375$  to  $\rho = 0.425$ , the lamellar phase has a directional ordering, as we shown in figure 2(ix). The region where we observe the oriented rippled lamellae was labeled VI-B. These lamellar structures, usually observed in amphiphilic molecules as in Janus particles<sup>53–55</sup>, were not observed in bulk for



our model of Janus nanoparticles. Therefore, this new structure is induced by the geometrical confinement. While in bulk the particles do not have any geometrical restriction, remaining in the micellae phase when the density is up to  $\rho = 0.50$ <sup>34</sup>, the confinement, associated to a high density, leads the dumbbells to aggregate in the lamellar cluster. The time evolution of the distinct lamellar phases is shown in figure 4. For lower temperatures, the entropic contribution to the free energy is not sufficient to change the initial configuration and the lamellae structure do not change with time, remaining disoriented, as shown in figure 4(A). However, for higher temperatures, the initially disordered configuration changes to the oriented rippled structure, as we can see in figure 4(B). This lamellar phase with a preferable orientation is characteristic of dumbbells systems with one or two monomer that interacts by a two length scale potential<sup>31,35</sup>, but at lower temperatures it is frustrated by the confinement.

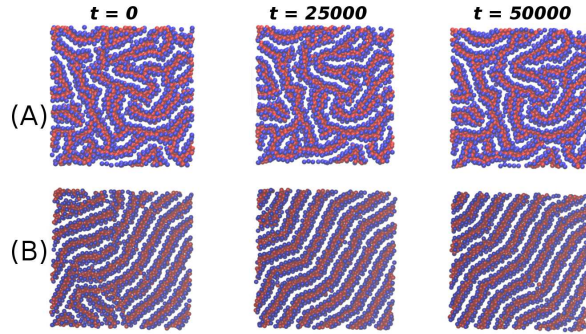


FIG. 4. Lamellar phase for the density  $\rho = 0.40$  at temperatures (A)  $T = 0.10$  and (B)  $T = 0.25$  at three distinct times: end of equilibration time ( $t = 0$ ), half of the production time ( $t = 25000$ ) and end of simulation ( $t = 50000$ ).

In the figure 5 we show the qualitative  $P_{||} \times T$  phase diagram for the confined system. The distinct micellae and lamellae regions are indicated. As discussed previously, new self-assembled structures are induced by the confinement. However, the aggregation region does not shift to higher or lower temperatures. Curiously, at the temperatures where we observe the oriented lamellae structure, for densities above  $\rho = 0.45$  the system has not a well defined micellar structure, and an amorphous phase is observed. This phase is a fluid with small diffusion. Taking the isotherm  $T = 0.25$  as reference, the pressure drops when  $\rho > 0.45$  and the system shows a reentrant fluid region. The plot of parallel diffusion coefficient as

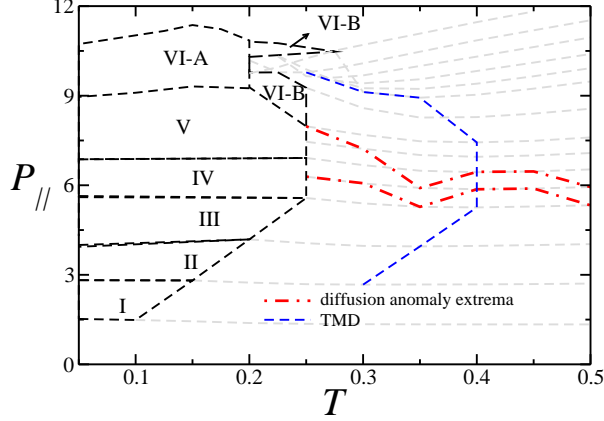


FIG. 5.  $P_{\parallel} \times T$  phase diagram for the confined Janus dimer system. The distinct micellae and lamellae regions discussed in the previous figures are indicated. The dashed gray lines are the isochores. The density anomalous regions is defined by the TMD line, and the diffusion anomaly region by the lines of maxima and minima diffusion.

function of density for some values of  $T$  is shown in figure 6. As we can see that for  $T = 0.25$  the system have  $D_{\parallel} \approx 0$  for  $\rho = 0.375, 0.40$  and  $0.425$ , and  $D_{\parallel}$  grows when  $\rho \geq 0.45$ , indicating a melting. The LRDF, showed in figure 7, also shows a decrease in the system structure, from the well structured lamellar phase to the fluid phase. This melting induced by the increase of density was already observed in colloidal glasses systems<sup>56–58</sup>, but was not observed in our bulk system.

The fluid phase also shows interesting properties, distinct from the bulk case. The first one is the density anomaly. As we can see, the isochores in figure 5 show a minimum. The dashed blue line, the so called TMD line, connects these minimum points. The density anomaly was observed for pure anomalous monomer and dimers (AA dimers)<sup>29,31</sup>, however was not present in the bulk Janus system<sup>34</sup>. The reentrant region, that occurs at higher densities, is located where the TMD line ends and splits the lammelar phase VI-B in two regions.

The bulk system has only diffusion anomaly, and it is preserved in the confined case. However, the diffusion extrema line for the confined system, defined by the red dot-dashed red line in the phase diagram, figure 5, have a temperature range larger than in bulk. Studies for confined anomalous fluids indicate that the TMD moves to lower temperatures for solvophobic confinement and higher temperatures for solvophilic confinement<sup>46,59,60</sup>. For the

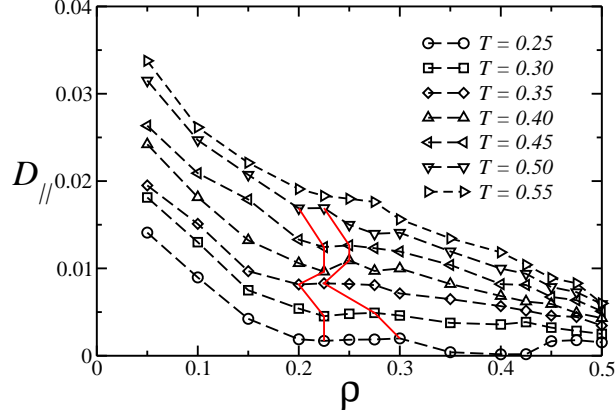


FIG. 6. Parallel diffusion  $D_{||}$  as function of density  $\rho$  for different temperatures. The red lines indicate the minima and maxima in the diffusion coefficient.

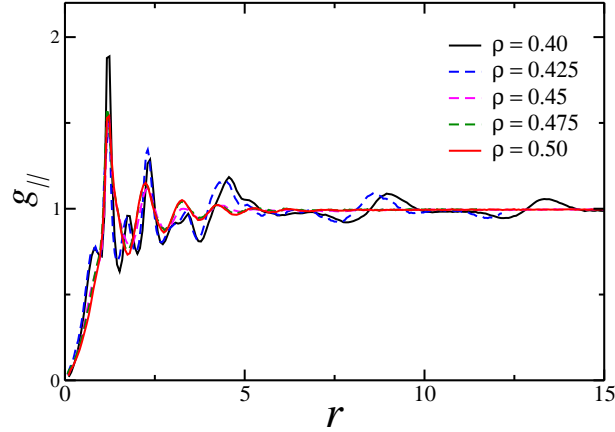


FIG. 7. Lateral radial distribution function (LRDF)  $g_{||}(r)$  for  $T = 0.25$ , showing the melting induced by the density increase.

bulk case, our hypothesis was that the TMD line was absorbed by the micellae region. Hence, since our confinement is solvophobic (the WCA potential is purely repulsive), is surprising that the TMD appears, moving to higher temperatures. This leads to the question: why the anomalies lines are shifted to higher temperatures?

Gavazzoni and co-authors<sup>32</sup> showed that the anisotropy can shift the solid-fluid phase boundary of dumbbells systems made only by A monomers. More than this, the work argues that the kinetic energy and, therefore, the temperature, has two contribution: the translational temperature and the non-translational temperature. Hence, the contribution

from the dimer rotations to the kinetic energy plays a significant role in this system behavior. In bulk, our Janus dumbbell can rotate freely in any direction - the only limitation are collisions with others dimers. However, the confinement imposes a constriction to the system. In our strongly confined system, with  $L_z = 4.0$  and  $\lambda = 0.8$ , not only the translation in  $z$ -direction is limited, but the combination of confinement with the competing interactions of Janus systems lead to a interesting phenomena. As the figure 6 shows, the diffusion coefficient is distinct from zero – so, the particles are moving in the parallel direction. In the figure 8(i) we show a frontal snapshot of the nanoparticles arrangement. As we can see, the particles are disordered - as expected for fluids. Notwithstanding, the side snapshot shows that in the  $z$ -direction the particles have a preferential position: the attractive B particles stay at the center, and the repulsive A particles are near the wall. Then, due the confinement and the Janus characteristics, the dimers are translating in the  $xy$ -plane, but without rotation. This places the A monomers side by side in the  $xy$ -plane, with a internal layer of attractive B monomers. This internal layer will act similar to a solvophilic wall, with the B monomers pulling one another. As consequence, the behavior is similar to water in hydrophilic confinement, and the anomalous region shifts to higher temperatures.

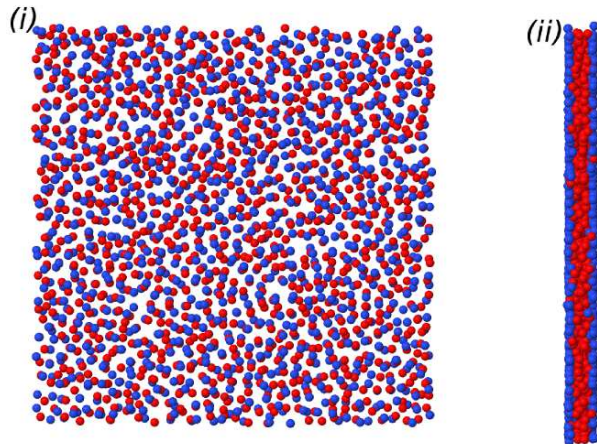


FIG. 8. Frontal (i) and side view (ii) of the system in the fluid region at  $T = 0.40$  and  $\rho = 0.30$ .

#### IV. CONCLUSION

We report the study of confined Janus nanoparticles. This system has special interest in the design of new material using the confinement to control the self-assembled structures.

We have found a rich variety of aggregates and micelles, including large micelles not observed in the bulk system. As well, two lamellae phases, with distinct orientations, were induced by the confinement. The oriented lamellae phase region in the  $P_{\parallel}T$  phase diagram is splitted by a reentrant fluid phase. This melting, induced by increasing the density, was not present in the bulk system as well.

Another feature that was not observed in the bulk system is the density anomaly. The combination of confinement effects with the competing interactions of Janus dimers shifts the TMD line to higher temperatures, rising the anomaly that was hidden inside the aggregation region for the bulk case. As well, the diffusion anomaly region increases, reaching higher temperatures.

Our results show that materials composed by the association of a monomer which can be modeled by a two length scale potential and a standard LJ monomer have an interesting and peculiar behavior.

## V. ACKNOWLEDGMENTS

The authors are grateful to Marcia C. Barbosa from Universidade Federal do Rio Grande do Sul for valuable and critical discussion. JRB thanks the Brazilian agency CNPq for the financial support.

## REFERENCES

- <sup>1</sup>K.-H. Roh, D. C. Martin and J. Lahann, *Nature Materials*, 2005, **4**, 759.
- <sup>2</sup>S. H. L. Klapp, *Curr. Opin. in Coll. and Inter. Sci.*, 2016, **21**, 76–85.
- <sup>3</sup>C. Casagrande, P. Fabre, E. Raphaël and M. Veyssié, *Europhys. Lett.*, 1989, **9**, 251–255.
- <sup>4</sup>D. M. Talapin, J.-S. Lee, M. V. Kovalenko and E. V. Shevchenko, *Chem. Rev.*, 2010, **110**, 389–458.
- <sup>5</sup>A. Eliskova, Z.-A. Li, C. Möller, M. Spasova, M. Acet, M. Farle, M. Kawasaki, P. Ercius and T. Duden, *Phys. Stat. Sol.*, 2011, **208**, 2437–2442.
- <sup>6</sup>F. Tu, B. J. Park and D. Lee, *Langmuir*, 2013, **29**, 12679–12687.
- <sup>7</sup>A. Walther and A. H. E. Müller, *Soft Matter*, 2008, **4**, 663–668.
- <sup>8</sup>A. Walther and A. H. E. Müller, *Chem. Rev.*, 2013, **113**, 5194–5261.

- <sup>9</sup>J. Zhang, E. Luijten and S. Granick, *Annu. Rev. Phys. Chem.*, 2015, **66**, 581–600.
- <sup>10</sup>T. Bickel, G. Zecua and A. Würger, *Phys. Rev. E*, 2014, **89**, 050303.
- <sup>11</sup>X. Ao, P. K. Ghosh, Y. Li, G. Schmid, P. Hänggi and F. Marchesoni, *Europhys. Lett.*, 2015, **109**, 10003.
- <sup>12</sup>Y. Yin, Y. Lu and X. Xia, *J. Am. Chem. Soc.*, 2001, **132**, 771–772.
- <sup>13</sup>V. Singh, C. Cassidy, P. Grammatikopoulos, F. Djurabekova, K. Nordlund and M. Sowwan, *J. Phys. Chem. C*, 2014, **118**, 13869–13875.
- <sup>14</sup>Y. Lu, Y. Yin, Z.-Y. Li and Y. Xia, *Nano Lett.*, 2002, **2**, 785–788.
- <sup>15</sup>K. Yoon, D. Lee, J. W. Kim and D. A. Weitz, *Chem. Commun.*, 2012, **48**, 9056–9058.
- <sup>16</sup>Y. Song, L. M. Klivansky, Y. Liu and S. Chen, *Langmuir*, 2011, **27**, 14581–14588.
- <sup>17</sup>Y. K. Takahara, S. Ikeda, S. Ishino, K. Tachi, K. Ikeue, T. Sakata, T. Hasegawa, H. Mori, M. Matsumura and B. Ohtani, *J. Am. Chem. Soc.*, 2005, **127**, 6271–6275.
- <sup>18</sup>J. Liu, G. Liu, M. Zhang, P. Sun and H. Zao, *Macromolecules*, 2013, **46**, 5974–5984.
- <sup>19</sup>Y. Liu, W. Li, T. Perez, J. D. Gunton and G. Brett, *Langmuir*, 2012, **28**, 3–9.
- <sup>20</sup>S. Whitelam and S. A. F. Bon, *J. Chem. Phys.*, 2010, **132**, 074901.
- <sup>21</sup>G. Munaò, D. Costa, A. Giacometti, C. Caccamo and F. Sciortino, *Phys. Chem. Chem. Phys.*, 2013, **15**, 20590.
- <sup>22</sup>G. Munaò, P. O’Toole, T. S. Hudson and F. Sciortino, *Soft Matter*, 2014, **10**, 5269.
- <sup>23</sup>G. Munaò, P. O’Toole, T. S. Hudson, D. Costa, C. Caccamo, F. Sciortino and A. Giacometti, *J. Phys. Cond. Matt.*, 2015, **27**, 234101.
- <sup>24</sup>G. Avvisati, T. Visers and M. Dijkstra, *J. Chem. Phys.*, 2015, **142**, 084905.
- <sup>25</sup>B. Liu, C. Zhang, J. Liu, X. Qu and Z. Yang, *Chem Comm*, 2009, **26**, 3871–3873.
- <sup>26</sup>P. A. Netz, F. W. Starr, M. C. Barbosa and H. E. Stanley, *Physica A*, 2002, **314**, 470.
- <sup>27</sup>T. Morishita, *Phys. Rev. E*, 2005, **72**, 021201.
- <sup>28</sup>S. Sastry and C. A. Angell, *Nature Mater.*, 2003, **2**, 739–743.
- <sup>29</sup>A. B. de Oliveira, P. A. Netz, T. Colla and M. C. Barbosa, *J. Chem. Phys.*, 2006, **124**, 084505.
- <sup>30</sup>A. B. de Oliveira, P. A. Netz, T. Colla and M. C. Barbosa, *J. Chem. Phys.*, 2006, **125**, 124503.
- <sup>31</sup>A. B. de Oliveira, E. Nevez, C. Gavazzoni, J. Z. Paukowski, P. A. Netz and M. C. Barbosa, *J. Chem. Phys.*, 2010, **132**, 164505.

- <sup>32</sup>C. Gavazzoni, G. K. Gonzatti, L. F. Pereira, L. H. C. Ramos, P. A. Netz and M. C. Barbosa, *J. Chem. Phys.*, 2014, **140**, 154502.
- <sup>33</sup>G. M. F. Saija, *Phys. Chem. Chem. Phys.*, 2016, **18**, 9484–9489.
- <sup>34</sup>J. R. Bordin, L. B. Krott and M. C. Barbosa, *Langmuir*, 2015, **31**, 8577–8582.
- <sup>35</sup>J. R. Bordin, *Physica A*, 2016, **459**, 1–8.
- <sup>36</sup>M. R. Khadilkar and F. A. Escobedo, *Soft Matter*, 2016, **12**, 1506.
- <sup>37</sup>Y. Iwashita and Y. Kimura, *Scientific Reports*, 2016, **6**, 27599.
- <sup>38</sup>S. H. Lee, E. Y. Fung, E. K. Riley and C. M. Liddell, *Langmuir*, 2009, **25**, 7193.
- <sup>39</sup>K. Muangnapoh, C. Avendaño, F. A. Escobedo and C. M. L. Watson, *Soft Matter*, 2014, **10**, 9729.
- <sup>40</sup>M. P. Kim and G.-R. Yi, *Frontiers in Materials*, 2015, **2**, 45.
- <sup>41</sup>G. Rosenthal and S. H. L. Klapp, *Int. J. Mol. Sci.*, 2005, **13**, 9431.
- <sup>42</sup>G. Rosenthal and S. H. L. Klapp, *J. Chem. Phys.*, 2011, **134**, 154707.
- <sup>43</sup>L. B. Krott, J. R. Bordin, N. Barraz Jr. and M. C. Barbosa, *J. Chem. Phys.*, 2015, **1**, 134502.
- <sup>44</sup>L. B. Krott, J. R. Bordin and M. C. Barbosa, *J. Phys. Chem. B*, 2015, **119**, 291–300.
- <sup>45</sup>J. R. Bordin, L. B. Krott and M. C. Barbosa, *J. Chem. Phys.*, 2014, **141**, 144502.
- <sup>46</sup>L. B. Krott and M. C. Barbosa, *Phys. Rev. E*, 2014, **89**, 012110.
- <sup>47</sup>P. Allen and D. J. Tildesley, *Computer Simulation of Liquids*, Oxford University Press, Oxford, 1987.
- <sup>48</sup>G. S. Kell, *J. Chem. Eng. Data*, 1967, **12**, 66.
- <sup>49</sup>C. A. Angell, E. D. Finch and P. Bach, *J. Chem. Phys.*, 1976, **65**, 3063–3066.
- <sup>50</sup>H.-J. Limbach, A. Arnold, B. A. Mann and C. Holm, *Comput. Phys. Commun.*, 2006, **174**, 704–727.
- <sup>51</sup>A. Arnold, O. Lenz, S. Kesselheim, R. Weeber, F. Fahrenberger, D. Roehm, P. Kosovan and C. Holm, *Meshfree Methods for Partial Differential Equations VI*, Springer Berlin Heidelberg, 2013, vol. 89, pp. 1–23.
- <sup>52</sup>P. Kumar, S. V. Buldyrev, F. W. Starr, N. Giovambattista and H. E. Stanley, *Phys. Rev. E*, 2005, **72**, 051503.
- <sup>53</sup>A. K. Khandpur, S. Foerster, F. S. Bates, I. W. Hamley, A. J. Ryan, W. Bras, K. Almdal and K. Mortensen, *Macromolecules*, 1995, **28**, 8796.

- <sup>54</sup>D. J. Beltran-Villegas, B. A. Schultz, N. H. Nguyen, S. C. Glotzer and R. G. Larson, *Soft Matter*, 2012, **10**, 4593.
- <sup>55</sup>Z. Preisler, T. Vissers, F. Smalenburg and F. Sciortino, *J. Chem. Phys.*, 2016, **145**, 064513.
- <sup>56</sup>L. Berthier, A. J. Moreno and G. Szamel, *Phys. Rev. E*, 2010, **85**, 060501.
- <sup>57</sup>D. Coslovich and A. Ikeda, *Soft Matter*, 2013, **9**, 6786.
- <sup>58</sup>J. C. Everts, N. Boon and R. van Roij, *Phys. Chem. Chem. Phys.*, 2016, **18**, 5211.
- <sup>59</sup>L. B. Krott and M. C. Barbosa, *J. Chem. Phys.*, 2013, **138**, 084505.
- <sup>60</sup>S. R.-V. Castrillon, N. Giovambattista, I. A. Aksay and P. G. . Debenedetti, *J. Phys.Chem. B*, 2009, **113**, 1438.